Millimeter-Wave Radio Channels vs. Synthetic Beamwidth

Ruoyu Sun, Camillo A. Gentile, Jelena Senic, Peter Vouras, Peter B. Papazian, Nada T. Golmie, and Kate A. Remley

Abstract

High-gain narrow-beam antennas or beamformed antenna arrays will likely be used in millimeter-wave (mmWave) bands and 5G to mitigate the high path loss. Since many multipath components may be excluded by the narrow beam, the mmWave radio channel (consisting of the transmit antenna, the propagation channels, and the receive antenna) strongly depends on the beamwidth, orientation, and shape of the narrow beam. In this article, a procedure is proposed to measure and model the channels vs. synthetic beamwidth. Based on experimental data collected at 60 GHz in an indoor hallway/lobby scenario, the results show that the number of multipath components and the delay dispersion of the channel are significantly reduced by the narrow beams. In addition, the path loss can be decreased by more than 20 dB with an optimized beam-center orientation. The impact of the study on future 5G mmWave system design is discussed, including frequency reuse, antenna design, receiver design, equalization, and link budget.

Introduction

With the explosion of data consumption during the last two decades, mobile networks suffer from limited availability of sub-6 GHz spectrum. On one hand, many new techniques are proposed to utilize and share the spectrum more efficiently. In March 2016, the Third Generation Partnership Project (3GPP) introduced Long Term Evolution Unlicensed (LTE-U) and LTE Assisted Access (LAA) in Release 13 to use the unlicensed industrial, scientific, and medical (ISM) bands to increase channel capacity. However, the increased capacity is very limited, and interference with other systems has become a critical issue. On the other hand, hundreds of times of spectrum in millimeter-wave (mmWave) bands are available. Migrating to mmWave bands is already on the way. In July 2016, the United States Federal Communications Commission (FCC) allocated 3.85 GHz of licensed spectrum near 28, 37, and 39 GHz for 5G mobile networks, and 7 GHz of unlicensed spectrum from 64–71 GHz that is adjacent to the existing 57–64 GHz ISM bands.

The radio propagation channel characteristics in mmWave bands are significantly different from those in sub-6 GHz bands. Millimeter-wave signals have high path loss and large Doppler shift. The first Fresnel zone, which includes more than 98 percent of the propagating energy, becomes very narrow due to the short wavelengths of mmWave signals; hence, diffraction is very weak. Reflections become rich since the dimensions of objects in real environments are much larger than the wavelength. Diffraction and scattering in sub-6 GHz bands will likely become reflections in mmWave bands. Penetration loss and shadowing loss are also very high for mmWave signals. To address these challenges in mmWave channels, researchers and engineers from universities, research institutes, companies, and government are designing channel measurement equipment, collecting data, and developing channel models. There are many leading organizations and projects working on mmWave and 5G channel models, including 3GPP, the International Telecommunication Union (ITU), the 5G mmWave Channel Model Alliance established by the National Institute of Standards and Technology (NIST), IEEE 802.11 working groups, and the New York University Wireless and mmWave Based Mobile Radio Access Network for 5G Integrated Communications (mmMAGIC).

The short wavelengths of mmWave signals enable deployment and integration of massive multiple-input multiple-output (MIMO) with dozens or hundreds of antenna elements in the handset. Therefore, high-gain narrow beams may be formed and steered in fifth generation (5G) and next-generation wireless systems. Effects of omnidirectional, wide-beam directional, and pencil beams are illustrated in Fig. 1. The brown dash-dotted circle denotes an omnidirectional antenna pattern; the red dotted line denotes a directional antenna pattern with half-power beamwidth (HPBW) of 30°; the blue solid line denotes a pencil-beam antenna pattern with HPBW of 3°.

The first-generation analog cellular network used frequency-division multiple access (FDMA). Time-division MA (TDMA) and code-division MA (CDMA) were introduced in 2G and 3G. The 4G LTE employs orthogonal frequency-division MA (OFDMA). Beam- or space-division MA (BDMA/SDMA) [1] is being discussed as a candidate access technique for 5G. Beam-division multiplexing (BDM) and beam-division duplexing (BDD) are also of great interest. Thus, the channel capacity of 5G may be increased by not only the new spectrum, but also massive MIMO and beam-division techniques.

High-gain narrow-beam antennas or beamformed antenna arrays will likely be used in mmWave bands and 5G to mitigate the high path loss. Since many multipath components may be excluded by the narrow beam, the mmWave radio channel strongly depends on the beamwidth, orientation, and shape of the narrow beam. The authors propose a procedure to measure and model the channels vs. synthetic beamwidth.

Ruoyu Sun is with CableLabs; Camillo A. Gentile, Jelena Senic, Peter Vouras, Peter B. Papazian, Nada T. Golmie, and Kate A. Remley are with the National Institute of Standards and Technology.

Digital Object Identifier: 10.1109/MCOM.2018.1800177

0163-6804/18/$25.00 © 2018 IEEE

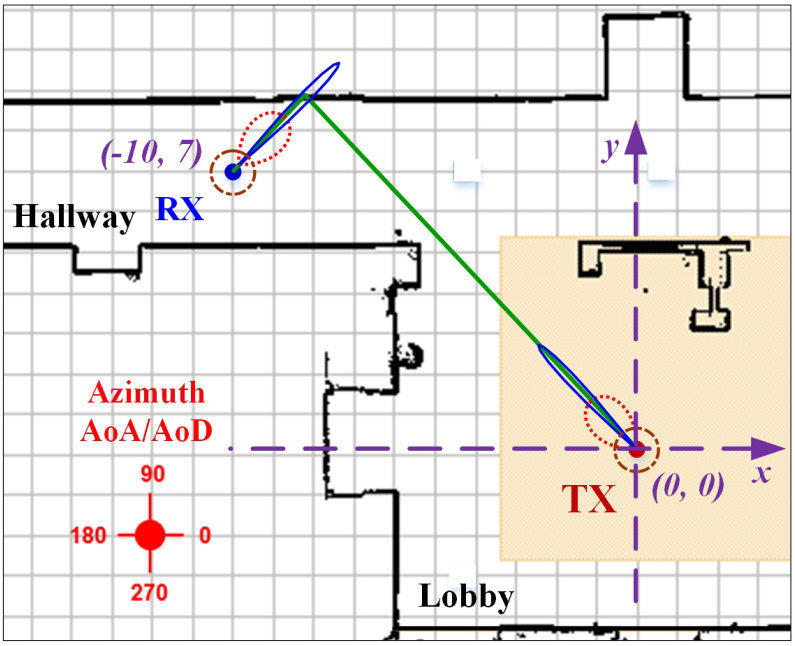

Figure 1. Antenna beamwidth impact on reception in a channel. The spacing on the grey grid is 1 m.

Traditionally, radio channels are studied with respect to distance, frequency, bandwidth, and scenario. As the utilization of high-gain, narrow-beam antennas in mmWave and 5G applications increases, knowledge of radio channels as a function of beamwidth is more and more critical. A beam is determined by orientation of the beam-center, the HPBW and the shape of the beam. By synthesizing various narrow beamwidths from an omni-directional measurement, engineers may study the impact of beamwidth on system design. The number and amplitude of multipath components (MPCs) will be affected by the spatial limits of the pencil-beam. Knowledge of channels vs. synthetic beamwidth is helpful for the next-generation wireless system antenna design, receiver design, and network planning.

The motivation of this article is to provide methods that study the channel with respect to synthetic beamwidth. The key contributions include summarizing angle of arrival (AoA) and angle of departure (AoD) sounding techniques, defining a synthetic beamwidth technique, and exploring its usefulness in modeling and design of spatial wireless systems. The novelty of this study extends to raising the question of beam-center selection and proposing four solutions. We present measurement results of path gain and root-mean-square delay spread (RMS-DS) as a function of synthetic beamwidth, which illustrate the procedure.

The AoA/AoD measurement techniques are summarized, and the synthetic beamwidth is defined. We discuss four methods of choosing the beam center. Empirical results are presented to quantitatively investigate the effect of synthetic beamwidth on RMS-DS and the effect of the choice of beam center on path gain. The potential impact of channels with narrow beams is discussed. We then present our conclusion.

Synthetic Beamwidth

AoA/AoD Channel Sounding Techniques

The AoA/AoD of MPCs can be measured by virtual array, electronic switched array, phased array, or other techniques. A single antenna (omnidirectional or directional) mounted on a mechanically moved [2] or rotated [3] translating stage is referred to as a virtual array. Channel snapshots are recorded dozens of times over the transmitter (TX) or receiver (RX) positions that are linearly moved or rotated on the translator with an increment of a fraction of a wavelength. The AoA/AoD is extracted by comparison of the phase differences between positions in a local area. Whether the virtual array is manually or automatically switched, the mechanical switching time and the time interval between two snapshots are typically on the order of seconds or more. This method generally measures a non-mobile scenario in which the channel is stationary (time-invariant) during the full channel scan. For example, for a virtual array having a grid of 30 positions in the X-direction and 30 positions in the perpendicular Y-direction, each position translation and its corresponding channel measurement takes 10 s. Thus, the channel needs to be stationary during 30 × 30 × 10 = 9000 s. The fastest virtual array sounder reported to date was designed by the Fraunhofer Heinrich Hertz Institute [4], which employs a high-speed spinning table with rotation speed of 625 rotations/min. In total, 1000 channel impulse responses (CIRs) could be recorded in a full rotation of 96 ms. The cost of a virtual array is low, and its calibration is easy.

An electronic switched array has multiple directional TX and RX antennas that are oriented in different directions. Only one pair of antennas is turned on at a time, and all combinations of antenna pairs are electronically switched. The AoA/AoD of an MPC can be extracted by comparison of delay and/or amplitude of the MPC that has arrived at different antennas. A full channel scan by a switched array can be done within a fraction of a millisecond depending on the delay span (maximum length in terms of delay) of the CIR, switching time, and switch rise time. Short switch times enable the measurement of high-mobility scenarios.

For example, the NIST 60 GHz sounder has 8 TX antennas and 16 RX antennas. Its CIR delay span from a single pair of antennas is 1023.5 ns. Each antenna has an amplifier that is electronically switched on and off. To avoid errors in estimating the CIR due to the amplifier's rise time, two CIRs are recorded, but only one is used in post-processing. A full channel scan takes only 1023.5 ns × 2 × 8 × 16 = 262 μs. Its reciprocal corresponds to a channel scan update rate of 3816 scans/s, which can measure a Doppler shift of up to 1908 Hz (based on the Nyquist criterion), corresponding to a TX-RX relative moving speed of approximately 34 km/h [5].

Phased arrays utilize a large number of antenna elements working simultaneously. Each element uses different amplitude and phase values, and the complex-combined pattern can be formed to create a high-gain narrow beam. The full channel scan could be as fast as the electronic switched array, but might be restricted by the digital signal processing (DSP) capability and response time.

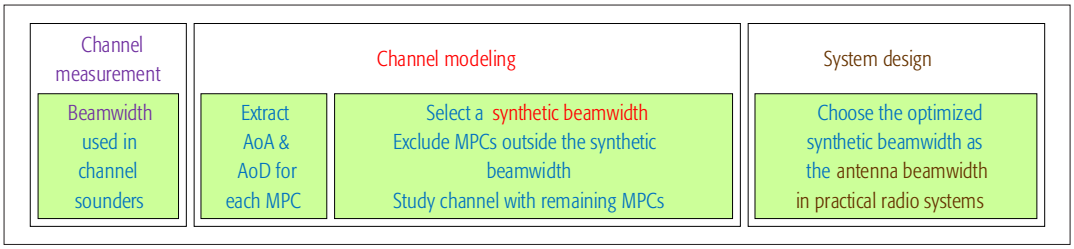

Figure 2. Antenna beamwidth vs. synthetic beamwidth.

By changing phase and magnitude coefficients, the phased array typically has more flexibility in beamwidth and gain during measurement than the virtual array and the switched array. It may also achieve higher dynamic range, but it is often restricted to a smaller set of scan-angle ranges. However, the virtual array could achieve such flexibility in post-processing. In [6], the authors reported a phased-array channel sounder at 27.85 GHz with 400 MHz bandwidth. Both TX and RX employ 8 × 2 antenna elements, which form a beam with vertical HPBW of 22° and horizontal HPBW of 12°. The minimum sweep time to cover 360° in azimuth is 1.44 ms.

The AoA/AoD can be measured by other techniques. A 16-feed lens array at 28 GHz frequency with 1 GHz bandwidth was developed by Sayeed in [7]. The boresight direction is adjusted by changing positions of 16 feeds. The lens array covers scan angles smaller than 180° in both azimuth and elevation with better resolution in the middle. A constant modulus chirp signal modulated by orthogonal frequency-division multiplexing (OFDM) corresponding to 64 tones is used to measure the channel. A channel scan takes 512 ns. Delay and angular resolutions are not reported.

After the data are collected by any of the measurement setups discussed above, the AoA/AoD of MPCs are extracted in post-processing by various algorithms. The authors of [8] use the space-alternating generalized expectation-maximization (SAGE) algorithm [9], which compares delay difference at multiple antennas for an individual MPC. The Communications Research Centre Canada (CRC) employs a modified CLEAN algorithm [10] that is based on an image-processing method. An iterative maximum likelihood estimation scheme, RIMAX, was used in [2] together with a path detection scheme. Other widely used algorithms include multiple-signal classification (MUSIC) and estimating signal parameters via rotational invariance technique (ESPRIT).

Definition of Synthetic Beamwidth

As illustrated in Fig. 2, there are three concepts of beamwidth:

1. Beamwidth of antenna hardware that is used in channel measurement
2. Synthetic beamwidth employed in channel modeling
3. Optimized beamwidth of an antenna for a given radio communication system

Antennas or antenna arrays used in propagation-channel measurements, whether a virtual array, switched array, phased array, or other technique, have certain physical beamwidths. These can be omnidirectional, or directional with wide beamwidth or narrow beamwidth.

		Euclidian	BP	GBRT	Scan
Requirement	Geometry and localization info	Yes	Yes	Yes	No
	3D strongest path scanning	No	No	No	Yes
Performance	LoS	Good	N/A	Good	Good
	NLoS	Bad	Moderate for wide synthetic beam; bad for pencil beam	Good	Very good

Table 1. Pros and cons of four beam centers.

In channel modeling, the AoA/AoD of MPCs are extracted from measured data in post-processing. These angles are randomly scattered in a large range that depends on the architecture of the sounder. To study a radio channel with a specific range of AoA/AoD, a synthetic beamwidth may be selected to study channel characteristics only with the MPCs inside that beamwidth, called a synthetic beamwidth.

Based on knowledge of channels corresponding to the synthetic beamwidth, an optimized beamwidth could be selected for a practical radio system, such as a 5G New Radio (NR) node-B (gNB). The rest of this article focuses on such synthetic beamwidths employed in channel modeling.

Synthetic Beam Pattern Filter

To exclude MPCs outside of the synthetic beamwidth, we can easily utilize a brick-wall filter that makes the power (or amplitude) of the MPCs outside the synthetic beamwidth zero and retains the original amplitude of the MPCs inside the synthetic beamwidth. However, no practical antenna has a beamwidth like a brick-wall filter. Thus, for realism, we filter the power by an antenna beam pattern defined by a shape function and its HPBW. The radiation pattern for a high-gain horn antenna or a beamforming array could be Gaussian, Cardioid, or other shapes. Scalar-feed horns, also termed corrugated conical horns, employed in the NIST channel sounders [11] have a Gaussian pattern. The gain of the 3D Gaussian beam pattern filter is an exponential function over synthetic HPBW, center of the beam in azimuth and elevation, and azimuth and elevation angles, as described in [8, Eq. 3].

Channel Modeling Procedure

Our procedure for studying synthetic beamwidth consists of the following steps:

1. Sound the channel with any type of antenna or array (e.g., omnidirectional, wide-beam, or narrow-beam antennas).

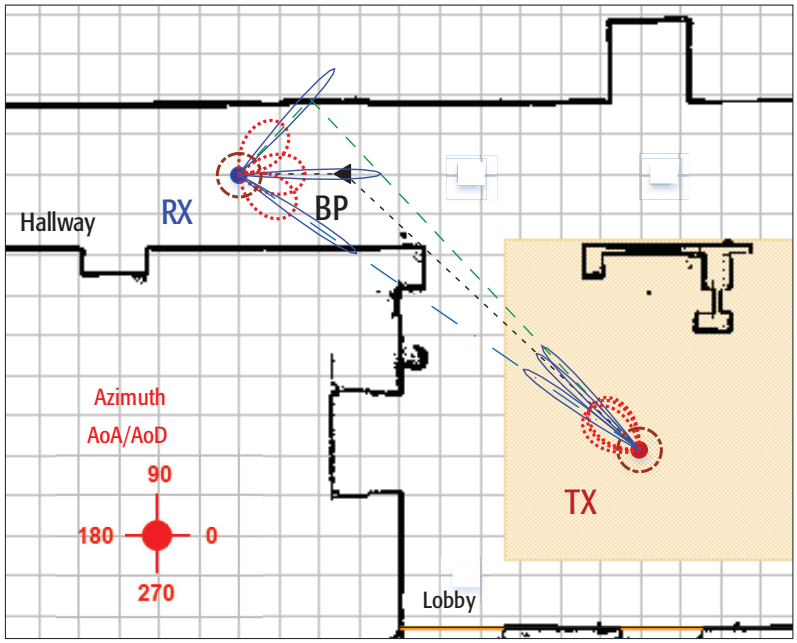

Figure 3. Center of the beams.

2. Extract AoA/AoD of each MPC.
3. Select beam center in azimuth and elevation.
4. Select a synthetic beamwidth, and generate a Gaussian (or other shape) pattern with the selected synthetic HPBW.
5. Exclude the MPCs outside the TX synthetic beamwidth by weighting the MPC power by the synthetic beam pattern.
6. Exclude the MPCs outside the RX synthetic beamwidth by weighting the MPC power by the synthetic beam pattern
7. Study channel characteristics and develop corresponding models for the selected synthetic beamwidth and beam centers
8. Select another synthetic beamwidth and beam center, and repeat steps 3 to 7.

For example, when we analyzed synthetic beamwidths from 1° to 360° with a 1° increment to investigate beam centers derived by four methods, steps 3 to 7 were repeated 1440 times.

Steering the Beam Center

The orientation, beam center, of the directional antenna plays a critical role in the received signal quality. Estimating AoA/AoD of the strongest path is important for narrow- or pencil-beam antennas. In this section, we discuss four beam-center selections for a synthetic beam and compare their requirements and performance, as listed in Table 1.

Euclidian Direction: The Euclidian direction utilizes geometry information from the propagation environment and locations of the TX and RX to find the direction of the direct path. The Euclidian direction is the straight line between TX and RX regardless of whether it is in line of sight (LoS) or non-LoS (NLoS) conditions. It is illustrated as the blue dash-dotted line in Fig. 3. The narrow beams of TX and RX steer toward the Euclidian direction. Its performance will be degraded when the direct path is obstructed, as shown in Fig. 3.

Direction toward the Break Point (BP): The black triangle in Fig. 3 is the break point, and the black dashed lines are the directions toward the BP. For distances shorter than the BP (RX on the right of BP), we have an LoS condition. When the RX is on the left of the BP we have an NLoS condition. In such a lobby/hallway environment, the RX beam points along the hallway (parallel to the walls) toward the BP, while the TX points toward the BP. In this case, the azimuthal AoA is a constant of 0° and the azimuthal AoD is 140.2°. In [12], the authors used the BP and the black dashed line to calculate the distance between TX and RX for a log-distance path loss model. This BP direction is only useful in NLoS conditions. It requires the geometry information of environment and locations of TX and RX.

Geometry-Based Reflection Tracking (GBRT): Based on the geometry of the environment and locations of TX and RX, we can use the optical ray-tracing method to find the direction of reflection. As the green solid line illustrates in Fig. 3, the reflection by the wall at the top of the figure is calculated and used as the beam center. This direction could also be extended to track double-bounce or multi-bounce MPCs. The wall at the bottom of the hallway in the figure has a rough surface. The GBRT method employed in this article does not consider surface roughness.

Scanning and Tracking the Strongest Direction: The three methods described above all require knowledge of the geometry of the environment and location information of the TX and RX, which may not be available to the real radio system. An alternative method for steering the beams is to scan the channel in three dimensions and find the strongest direction in real time. This direction is, ideally, very similar to the GBRT direction, shown by the green solid line in Fig. 3 for the given TX and RX positions. Such scanning costs power, time, and computational resources in both the TX and the RX.

Experimental Results: Channel Characteristics vs. Synthetic Beamwidth

Experimental data were collected in the Katharine Blodgett Gebbie building on the NIST Boulder Laboratories campus. The map and coordinates are depicted in Fig. 1. The width of the hallway is 4 m. The lobby is 13 × 13 m. The TX was at the origin (0, 0), and the RX moved along a straight line from (0, 7) to (–24, 7) units in meters. The TX height was 2.5 m, and the RX height was 1.6 m. The direct path was available when the TX-RX distance ranged from 7.1 to 13 m. From 13 to 19 m, single-reflection (by the wall on the top of Fig. 1) was the dominant path. From 19 to 25 m, double-reflection (first by the top wall and then by the wall on the bottom of the hallway) was the dominant path. A detailed description of the scenario and test method was presented in [8]. Our channel sounder hardware is calibrated using a back-to-back procedure using predistortion filters [5]. Calibrations of frequency drift and phase noise are in process. Detailed information on the sounder design, calibration, performance evaluation, and data processing are provided in [5, 11].

The channel measurement system utilizes a pseudorandom (PN) sequence with length of 2047 bits. The bit rate is 2 Gb/s, which corresponds to a delay resolution of 0.5 ns. The center frequency is 60.5 GHz. Scalar-feed horns have 18.1 dBi gain and 22.5° HPBW in both azimuth and elevation. The transmitted power is 20 dBm.

As described earlier, 8 TX antennas and 16 RX antennas are electronically switched to cover 180° at TX and 360° at RX in azimuth and 90° in elevation. Dozens to over 100 MPCs are extracted by the SAGE algorithm for a full channel scan. Each MPC is described by power, delay, AoA, and AoD in azimuth and elevation. The AoA (AoD) of the MPCs are extracted by comparing the delay difference of the signal received (transmitted) by five adjacent antennas using the SAGE algorithm. The angular resolution is 1°. Based on a comparison with geometry of the environment, the error of the angular estimation is approximately 2° [8].

Delay Dispersion vs. Synthetic Beamwidth

The experimental RMS-DS value changes with the synthetic beamwidths are presented in this subsection. The AoA and AoD in azimuth and elevation of the strongest MPC, based on the results from step 2 earlier, are used as the beam centers, as determined by the scanning method. An example of azimuth AoA beam center over distance results was provided in [8]. From the channel modeling procedure provided earlier, the power of each MPC is changed by a Gaussian beam pattern filter based on the AoA/AoD of the MPC. The RMS-DS is calculated from the power and delay of MPCs with power above a multipath threshold of 25 dB relative to the strongest MPC [8]. The RMS-DS is estimated over synthetic beamwidths ranging from 1° to 360° with an increment of 1°.

Results are shown in Fig. 4. For clarity, only RMS-DS results with synthetic beamwidths of 360°, 30°, 15°, and 3° are shown. The corresponding maximum RMS-DS values are 14.9, 6.7, 6.0, and 1.4 ns, and the median RMS-DS values are 3.6, 0.2, 0.1, and 0.02 ns. The RMS-DS values for synthetic beamwidths of 30° and 15° are higher in the single-reflection region than in the LoS region. This is because the direct path in the LoS region was obstructed in the single-bounce region. However, this is not observed for a beamwidth of 3°. This is because the reflections from the top wall of the hallway are a cluster of MPCs due to wall roughness. The angles of these MPCs are scattered a few degrees apart. These MPCs are likely partially excluded by the 3° beamwidth. This is illustrated by a 3D plot of azimuthal AoA vs. distance vs. power provided in [8]. The RMS-DS results for all synthetic beamwidth values increased when entering the double-bounce region, as expected. In [13], RMS-DS results measured by an omnidirectional antenna and a horn antenna show a similar trend of decreasing RMS-DS with beamwidth.

Choice of Beam Centers vs. Path Gain

Path gain was computed with the total power of all MPCs filtered by the Gaussian beam pattern. An example of results of path gain over distance with synthetic beamwidth of 30? is depicted in Fig. 5 illustrating the difference in path gain when the beam center was derived in four ways. The scanning method always achieves the largest path gain for all distances. The path gains for the Euclidian and GBRT methods in the LoS region are identical, and very similar to the scanning method. In NLoS conditions, the scanning and GBRT provide channels having higher path gains than the other two methods, and the BP is slightly better than the Euclidian. The difference between the

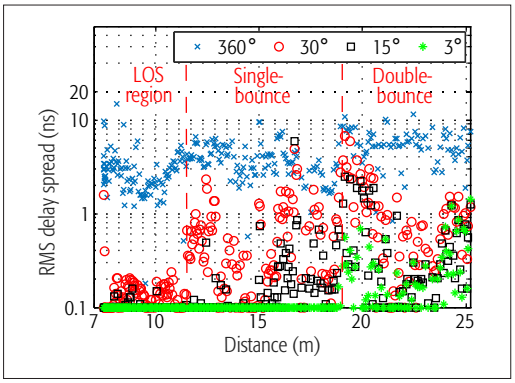

Figure 4. RMS-DS (log scale) and synthetic beamwidth vs. distance. For clarity, any RMS-DS values smaller than 0.1 ns are set to 0.1 ns.

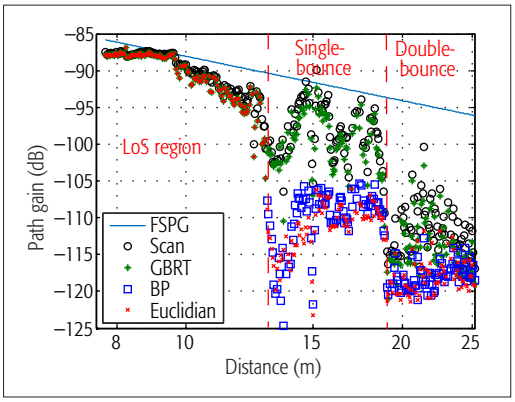

Figure 5. Path gain vs. distance (log scale) for the four beam center algorithms with a synthetic beamwidth of 30°. FSPG denotes free-space path gain.

scanning and GBRT in the single-bounce region is, on average, 1.3 dB with a maximum value of 4.7 dB. Their difference in the double-bounce region increases to 2.2 (average) and 5.7 (max) dB. The difference is due to factors such as angular estimation errors that are smaller than 2°, and inaccurate geometry information of the environment and roughness of the wall surface.

Path gain results for other synthetic beamwidth values were also investigated. Path gain results are identical for four beam center choices when the beamwidths are close to 360°, and the difference between center choices increases as the synthetic beamwidth decreases. For beamwidths smaller than 10°, the Euclidian/GBRT methods have path gains smaller than the scanning methods in the LoS condition. Again, this is due to angular estimation errors and inaccurate geometry information. For a synthetic beamwidth of 5°, the path gain difference between the Euclidian/GBRT and scanning methods is, on average, 9.1 dB with a maximum value of 23.4 dB. This indicates that, for narrow beamwidth, significant loss in path gain may be expected for only minor orientation errors, which is also observed in the measurement reported in [13].

Synthetic Beamwidth Effects on Other Channel Characteristics

Other channel characteristics are affected by beamwidth. Small-scale fading introduces deep nulls in both the time and frequency domains that

The beamwidth will impact future wireless system design and many aspects of system performance. For example, using the techniques presented here in practical next-generation radio-system design, an optimized beamwidth and boresight center could be selected based on the requirements and scenarios for the system's antennas or beamforming arrays.

reduce the availability of signals at the receivers. The magnitude of fading is expected to decrease with fewer MPCs due to narrower beamwidths. Inter-frequency cross-correlation that evaluates interference between in-band carriers is also expected to change over the beamwidth.

Since BDMA/BDM/BDD may be used in next-generation wireless systems, the interference between beams needs to be evaluated. Such interference can be evaluated by cross-correlation between signal strength of two beams (e.g., the direct path and wall reflection), where the signal strength is complex combined by all MPCs within the synthetic beamwidth. Hence, the inter-beam interference is a function of synthetic beamwidth and separation between the center of the beams.

Additionally, in antenna array design, the gain of each antenna element and spatial separation between elements is likely positively correlated. Their trade-off could be investigated by synthetic beamwidth and corresponding spatial correlation.

Impact and Applications

The mmWave channels created by the use of various synthetic beamwidths have been discussed in previous sections. As illustrated in these results, the beamwidth will impact future wireless system design and many aspects of system performance. For example, using the techniques presented here in practical next-generation radio system design, an optimized beamwidth and boresight center could be selected based on the requirements and scenarios for the system's antennas or beamforming arrays. Potential interference between adjacent beams (users) could then be estimated. These techniques will also be helpful for BDMA/BDM/BDD or multi-user MIMO (MU-MIMO) design.

Moreover, as the number of MPCs is decreased when employing narrow-beam antennas, delay dispersion and hence inter-symbol interference (ISI) are significantly mitigated. Consequentially, achieving a faster symbol rate may be possible. Many techniques used at the RX to mitigate multipath may no longer be necessary, including the Rake receiver and equalization. The overhead due to the cyclic prefix used in OFDM could be eliminated. One of the significant advantages of OFDM is dividing a wideband channel into multiple flat-fading narrowband channels to avoid frequency-selective fading and ISI. With narrow-beam antennas, use of OFDM with its high peak-average power ratio may be reconsidered.

The narrowband small-scale fading in both the time domain and frequency domain is expected to be much milder with a reduced number of MPCs. The short link range in mmWave bands due to high path loss is compensated for by both high antenna gain and mild fading. The ping-pong handover issue at the edge of cells could also be improved. The accuracy of localization might be improved by both narrow angles and less fluctuating RX power levels. Spatial diversity and cyclic delay diversity (CDD) used in LTE networks may not be needed.

Finally, both inter- and intra-frequency interference could be reduced by narrow beams, which improves the frequency reuse factor in cellular networks, increasing capacity and spectrum efficiency. Comprehensive knowledge of channels vs. synthetic beamwidth provides quantitative estimation for system designers to address these issues.

Conclusion

In this article, we define a synthetic beamwidth technique that may be used for channel modeling. The method is distinct from the antenna beamwidth employed in channel sounding and practical radio systems. A Gaussian beam pattern as a function of the synthetic HPBW and beam centers were defined to filter the MPCs outside the selected synthetic beamwidth. Selection of the beam centers is discussed. The AoA/AoD channel sounding techniques are summarized. A procedure describing how to sound and model channels vs. synthetic beamwidth is presented. The potential impact of the narrow-beam channel knowledge on future radio system design is discussed including frequency reuse, link budget, equalization, and BDMA.

We present measurement results at 60 GHz in a hallway/lobby environment that illustrate the significance of considering synthetic beamwidth and validate the proposed methodology. The RMS-DS decreased dramatically from 15 ns to almost 1.4 ns (maximum values) as the synthetic beamwidth decreased from 360° to 3°. Optimized beam center selection achieved up to over 20 dB path gain as compared to other center selection methods with 30° beamwidth. Future work includes analysis of small-scale fading, inter-frequency correlation, inter-beam correlation, and other channel characteristics vs. synthetic beamwidth.

References

[1] D. H. Cho *et al.*, "Beam Division Multiple Access System and Method for Mobile Communication System," Patent WO2009041759A1, 2009.

[2] J. Salmi and A. F. Molisch, "Propagation Parameter Estimation, Modeling and Measurements for Ultrawideband MIMO Radar," *IEEE Trans Antennas and Propagation*, vol. 59, no. 11, Nov. 2011, pp. 4257–67.

[3] G. R. MacCartney *et al.*, "Indoor Office Wideband Millimeter-Wave Propagation Measurements and Channel Models at 28 and 73 GHz for Ultra-Dense 5G Wireless Networks," *IEEE Access*, vol. 3, 2015, pp. 2388–424.

[4] M. Schmieder *et al.*, "Measurement and Characterization of 28 GHz High-Speed Train Backhaul Channels in Rural Propagation Scenarios," *2018 12th Euro. Conf. Antennas and Propagation*, London, U.K., 9–13 Apr. 2018.

[5] R. Sun *et al.*, "Design and Calibration of a DoubleDirectional 60 GHz Channel Sounder for Multipath Component Tracking," *11th Euro. Conf. Antennas and Propagation*, Paris, France, 19–24 Mar. 2017, pp. 3336–40.

[6] C. U. Bas *et al.*, "A Real-Time Millimeter-Wave Phased Array MIMO Channel Sounder," *IEEE VTC-Fall 2017*, Sept. 2017, Toronto, ON, Canada, pp. 1–6.

[7] A. Sayeed *et al.*, "Indoor Channel Measurements Using a 28GHz Multi-Beam MIMO Prototype," *IEEE VTC-Fall 2016*, Montreal, QC, Canada, 18–21 Sept. 2016, pp. 1–5.

[8] R. Sun *et al.*, "Angle- and Delay-Dispersion Characteristics in a Hallway and Lobby at 60 GHz," *2018 12th Euro. Conf. Antennas and Propagation*, London, U.K., 9–13 Apr. 2018, pp. 1–5.

[9] J. A. Fessler and A. O. Hero, "Space-Alternating Generalized Expectation-Maximization Algorithm," *IEEE Trans. Signal Proc.*, vol. 42, no. 10, Oct. 1994, pp. 2664–77.

[10] Y. de Jong *et al.*, "2.4 to 61 GHz Multiband Double-Directional Propagation Measurements in Indoor Office Environments," *IEEE Trans. Antennas and Propagation*, vol. 66, no. 9, Sept. 2018, pp. 4806-20.

[11] P. B. Papazian *et al.*, "A Radio Channel Sounder for Mobile Millimeter-Wave Communications: System Implementation and Measurement Assessment," *IEEE Trans. Microwave Theory and Techniques*, vol. 64, no. 9, Sept. 2016, pp. 2924–32.

[12] J. Senic *et al.*, "Analysis of E-Band Path Loss and Propagation Mechanisms in the Indoor Environment," *IEEE Trans. Antennas and Propagation*, vol. 65, no. 12, Dec. 2017, pp. 6562–73.
[13] J. Lee *et al.*, "Field-Measurement-Based Received Power Analysis for Directional Beamforming Millimeter-Wave Systems: Effects of Beamwidth and Beam Misalignment," *ETRI J.*, vol. 40, no. 1, Feb. 2018, pp. 26–38.

Biographies

Ruoyu Sun [M'13, SM'17] received his B.S. degree from Tianjin University in 2004, his M.S. degree from Beijing Jiaotong University in 2007, and his Ph.D. degree from the University of South Carolina in 2015, all in electrical engineering. He is a lead architect at CableLabs, Louisville, Colorado. He was an electronics engineer at the National Institute of Standards and Technology (NIST), Boulder, Colorado. His research interests include radio propagation channel measurements and modeling.

Camillo Gentile [M'01] received his B.S. and M.S. degrees from Drexel University in 1996 and his Ph.D. degree from Penn State University in 2001, all in electrical engineering. He joined the NIST in 2001. He has authored over 60 peer-reviewed papers and a book on geolocation techniques. In 2015, he became a project leader. His current interests include channel modeling and physical-layer modeling for millimeter-wave communication systems.

Jelena Senic received her B.S. and M.S. degrees in electrical engineering from the School of Electrical Engineering, University of Belgrade, Serbia, in 2009 and 2010, respectively. Since January 2015, she has been a guest researcher at NIST. Her current research interests include millimeter-wave communications, measurements of signal propagation, and channel modeling for 5G. The team she works with received the Best Measurement Paper Award at EuCAP 2017.

Peter Vouras received his B.A. degrees in economics and foreign affairs from the University of Virginia, his B.S. degree in electrical and computer engineering from George Mason University, and his M.S.E. degree from Johns Hopkins University, Baltimore, Maryland. In 1996, he joined the Radar Division of the Naval Research Laboratory, and since October 2017 he has been with the Wireless Networks Division of NIST, Gaithersburg, Maryland.

Peter Papazian [SM'98] received his B.S. in physics at the State University of New York Stonybrook in 1973 and an M.S. degree from Colorado School of Mines in 1979. Currently, he is the 5G Millimeter-Wave Channel Sounder project leader at the NIST Communications Technology Laboratory in Boulder, Colorado. The purpose of this research is to conduct millimeter-wave radio channel propagation measurements to support model and standards development for 5G radio systems.

Nada Golmie received her Ph.D. in computer science from the University of Maryland at College Park. She is currently the chief of the wireless networks division in the Communications Technology Laboratory at NIST. Her research in media access control and protocols for wireless networks has led to over 100 technical papers presented at professional conferences and in journals. She serves as a Co-Chair for the 5G mmWave Channel Model Alliance.

Kate A. Remley is the leader of the Metrology for Wireless Systems Group at NIST, where her research includes improved calibrations and standardized measurements of microwave and millimeter-wave wireless systems. She received the Department of Commerce Bronze and Silver Medals and is a member of the Oregon State University Academy of Distinguished Engineers. She has chaired various MTT-S committees, was Editor-in-Chief of *IEEE Microwave Magazine*, and served as A Distinguished Lecturer for the IEEE EMC Society.